Ocean and Coastal Management 217 (2022) 105984

Contents lists available at ScienceDirect

Ocean and Coastal Management

journal homepage: www.elsevier.com/locate/ocecoaman

Modelling of annual sand transports at the Dutch lower shoreface

Bart Grasmeijer [a,c,*], Bas Huisman [a], Arjen Luijendijk [a,e], Reinier Schrijvershof [a,f], Jebbe van der Werf [a,d], Firmijn Zijl [a], Harry de Looff [b], Wout de Vries [b]

[a] Deltares, Boussinesqweg 1, 2629 HV Delft, The Netherlands
[b] Rijkswaterstaat, Griffioenlaan 2, 3526 LA Utrecht, The Netherlands
[c] Utrecht University, Princetonlaan 8a, 3584 CB Utrecht, The Netherlands
[d] University of Twente, Drienerlolaan 5, 7522 NB Enschede, The Netherlands
[e] Delft University of Technology, Stevinweg 1, 2628 CN Delft, The Netherlands
[f] Wageningen University and Research, Droevendaalsesteeg 3, 6708 PB Wageningen, The Netherlands

ARTICLE INFO

Keywords:
Coastal Genesis 2.0
Dutch lower shoreface
Sand transport
Modelling

ABSTRACT

Dutch coastal policy aims for a safe, economically strong and attractive coast. This is achieved by maintaining the part of the coast that support these functions; the coastal foundation. The coastal foundation is maintained by means of sand nourishments. Up to now, it has been assumed that net transports across the coastal foundation's offshore boundary at the 20 m depth contour are negligibly small. In the framework of the Coastal Genesis 2.0 program we investigated sand transports across this boundary and across other depth contours at the lower shoreface.

This paper presents a computationally efficient approach to compute the annual sand transport rates at the Dutch lower shoreface. It is based on the 3D Dutch Continental Shelf Model with Flexible Mesh (3D DCSM-FM), a wave transformation tool and a 1DV sand transport module. We validate the hydrodynamic input against field measurements and present flow, wave and sand transport computations for the years 2013–2017.

Our computations show that the net annual sand transport rates along the Dutch coast are determined by peak tidal velocities (and asymmetry thereof), density driven residual flows, wind driven residual flows and waves.

The annual mean alongshore transports vary along the continuous 20 m depth contour. The computed total cross-shore transports are onshore directed over the continuous 20 m, 18 m and 16 m depth contours and increase with decreasing water depth.

The effect of density difference and wind on the 3D structure of the flow and on the sand transports cannot be neglected along the Dutch lower shoreface. Our computations show that excluding the effect of density results in a significant decrease of the onshore directed transports. Also switching off wind largely counteracts this effect.

The net cross-shore transport is determined by a delicate balance between gross onshore and offshore transports, where wave conditions are important. We show an example for Scheveningen where the net cross-shore transport is onshore directed when including all wave conditions but would be offshore directed when excluding waves higher than 3.5 m. In contrast, at Callantsoog the highest waves contribute more to the offshore directed transports. These results suggest that storm conditions play an important role in the magnitude and direction of the net annual transport rates at the lower shoreface.

1. Introduction

Dutch coastal policy aims for a safe, economically strong and attractive coast. This is achieved by maintaining the part of the coast that support these functions; the coastal foundation (Mulder et al., 2011). The offshore boundary of the coastal foundation is presently taken at the NAP -20 m depth contour (NAP = Dutch Ordnance Level corresponding approximately with Mean Sea Level (MSL)). The onshore boundary is formed by the landward edge of the dune area (closed coast) and by the tidal inlets (open coast). The borders with Belgium and Germany are the lateral boundaries (Fig. 1). The coastal foundation is maintained by means of sand nourishments; the total nourishment volume is approximately 12 million m^3/year since 2000.

* Corresponding author at: Deltares, Boussinesqweg 1, 2629 HV Delft, The Netherlands.
E-mail address: bart.grasmeijer@deltares.nl (B. Grasmeijer).

https://doi.org/10.1016/j.ocecoaman.2021.105984
Received 20 April 2021; Received in revised form 9 July 2021; Accepted 24 November 2021
Available online 29 December 2021
0964-5691/© 2021 The Author(s). Published by Elsevier Ltd. This is an open access article under the CC BY license (http://creativecommons.org/licenses/by/4.0/).

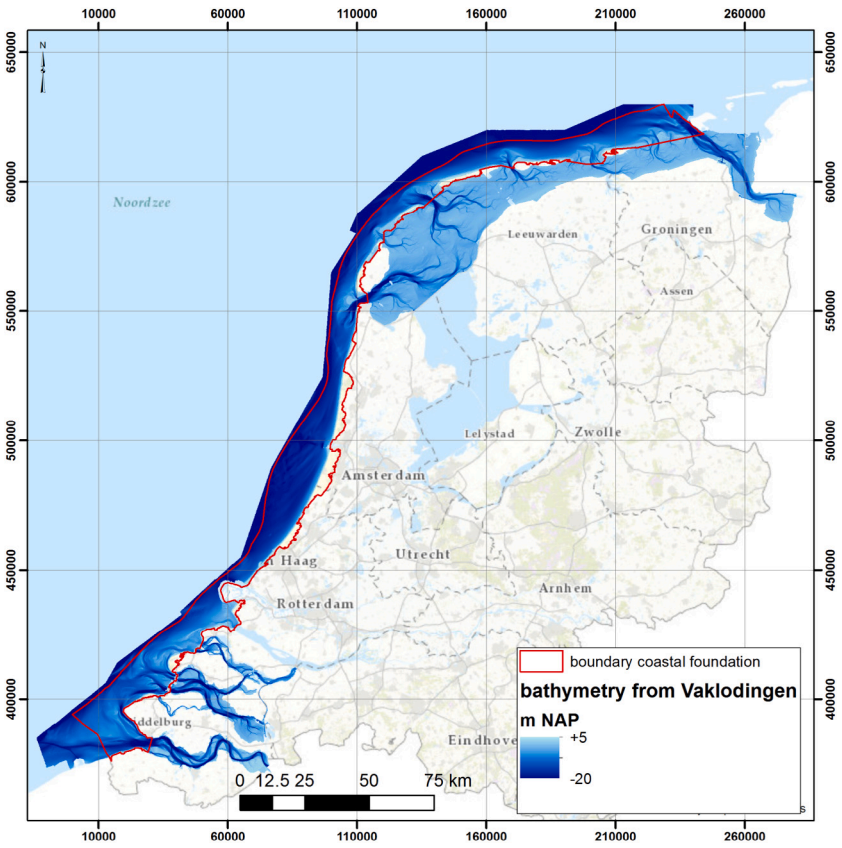


Fig. 1. Coastal foundation on top of bathymetry from measurements between 2009 and 2014.

Up to now, it has been assumed that net transports across the coastal foundation's offshore boundary at the 20 m depth contour are negligibly small. However, Hinton and Nicholls (2007) suggest that the lower shoreface morphodynamics is related to onshore supply of sand to the active zone and that the upper, middle and lower shoreface are coupled. This has widespread significance for understanding long-term coastal evolution and this paper provides new insights on this subject based on process-based model computations.

The shoreface is the active littoral zone off the low water line between the shore and the continental shelf. We define the upper shoreface as the beach and surf zone with breaking waves and breaker bars between the waterline and approximately the NAP -8 m depth contour with mean bed slopes varying between 1:50 to 1:200. We define the lower shoreface as the zone between approx. the NAP -8 m and NAP -20 m depth contours with typical bed slopes between 1:200 and 1:1000, and where sand ridges may be present.

The effects due to wave energy dissipation are dominant in the upper shoreface. Transport rates are relatively large and the morphological response time is fast, i.e. on the scale of events. The lower shoreface is the zone where the mixed action of shoreface currents (tide, density, wind) and shoaling and refracting waves is predominant. Transport rates are relatively small and hence the lower shoreface undergoes relatively slow adaptations, i.e. years to decades.

Anthony and Aagaard (2020) provide a review of research on the morphodynamics of the lower shoreface and the potential sediment exchanges between the lower shoreface and the upper shoreface and beach. Aagaard et al. (2004) linked long-term (decadal) shoreface profile development and event-scale process measurements and documented a net long-term onshore-directed sediment transport from the lower shoreface through the surf zone and to the subaerial beach/dunes at a gently sloping barrier on the Danish North Sea coast. Aagaard (2014) used field measurements of suspended sediment load and cross-shore transport on the lower shoreface to derive a model for sediment supply from the lower to the upper shoreface at large spatial and temporal scales. Patterson and Nielsen (2016) analyse measured 46 year changes in lower shoreface bathymetry to quantify rates of net shore-normal sand transport in 10–20 m depths at northern Gold Coast, Australia.

Van der Spek et al. (2022) give an overview of the lower shoreface of the Dutch Coast. Important modelling research has been done in 1990's in the framework of the first Coastal Genesis research program of Rijkswaterstaat. Roelvink and Stive (1991) and Van Rijn (1997) published research on the sediment transport of the Holland coast (between Hoek van Holland and Den Helder). In both studies, the yearly averaged transport was computed for a number of coast-normal transects. Important finding in these earlier studies is that the net sand transport on the Holland shoreface is determined by various subtle effects such as a density-gradient driven current but also that storm events play an important role and that a changing wave climate has a relatively big effect on the net transports. Van Rijn (1997) argued that the net cross-shore transports are the result of a delicate balance between the various onshore and offshore components (density- and wind-driven flow, wave boundary layer streaming, wave skewness, return flow) and that most of these components could not be represented with sufficient accuracy at that time. Therefore, he made an extensive sensitivity study to come up with variation ranges of the net transport. He reported net cross-shore transports of 0, 10, 15 and 5 m^3/m/year (shoreward) at 20 m water depth near Scheveningen, Noordwijk, Egmond an Callantsoog, respectively. The variation range was $\pm$ 10 m^3/m/year for all locations.

Stive et al. (1992) studied the seaward extent and the rate of morphodynamic activity across the active zone. They distinguished different time and length scales on this topic and concluded that at they would require modelling on a time scale longer than could be handled by process-based models at that time. They had to fall back on behaviour oriented models. Since then, improved computer techniques facilitated the development of large scale 2D models of the Dutch

coast. Van der Werf and Giardino (2009), Van der Hout et al. (2009) and Van der Spek et al. (2015) computed the hydrodynamics, sediment transport and morphodynamics along the Dutch coast with a 2D model. The predicted hydrodynamics and sediment transport along the Holland Coast and the Texel Inlet compared quite well with reference studies. A recent study of the large-scale sediment transport along the Dutch coast is from Knook (2013). He analysed cross-shore sediment transport rates at various depths on the lower shoreface of the Holland coast. This analysis was based on computations with the Unibest-TC model, which makes the approach similar to the one by Roelvink and Stive (1991) and Van Rijn (1997), although density-gradient effects were not accounted for.

The earlier work has mainly focused on the Holland coast between Hoek van Holland and Den Helder without the effects of tidal inlets or estuaries. The computations in these earlier studies were based on cross-shore profile models (2DV) or horizontal depth-averaged models (2DH) and required schematizing wave and current conditions based on results from large scale models or excluding effects such as salinity and 3D circulation in order to keep the computation time limited. However, 3D circulation patterns by e.g. fluid density gradients play an important role for the total cross-shore transport rate at water depths deeper than about 8 m (e.g. Van Rijn (1997)).

Process-based 3D modelling without simplifications, schematization or reduction of the hydrodynamic input and using models validated with field measurements to study the transport processes along the entire Dutch coast has not been done before. We developed a computationally efficient 3D modelling approach for this purpose.

In this paper, we describe the set-up and validation of such a modelling system and present results of the flow, wave and transport calculations based on this approach. We illustrate the cross-shore variation, the effects of density and wind and the relative contribution of different wave conditions.

2. Datasets and methods

We developed a computationally efficient approach to compute the annual sand transport rates at the Dutch lower shoreface. It is based on the 3D Dutch Continental Shelf Model with Flexible Mesh (3D DCSM-FM) of the entire Dutch coast (Zijl et al., 2018; Grasmeijer, 2018; Grasmeijer et al., 2019), a wave transformation tool and a 1DV sand transport module.

2.1. The 3D Dutch Continental Shelf Model-Flexible Mesh (3D DCSM-FM)

The 3D DCSM-FM model is an advanced 3D model for the computation of water levels, currents, salinities and temperatures in the greater North Sea. It is used for operational water and coastal management, and for further research. The model combines currents, water temperature and salinity with water levels (tide and storm surge). Both short-term (days/weeks/months) and long-term (years) developments can be clearly assessed, at both local (10–100 km) and large scales (100–10,000 km). The model provides insights into the fate and interactions of complex natural phenomena in coastal waters and the open sea. It covers the Northwest European Continental Shelf, which includes the entire North Sea from the Irish Sea to the Baltic Sea and from the coast of Northern Spain to the coast of Scandinavia.

The 3D DCSM-FM model is built in D-Flow Flexible Mesh (D-Flow FM) which is a hydrodynamic simulation program developed by Deltares. D-Flow FM is a multi-dimensional (1D, 2D and 3D) hydrodynamic (and transport) simulation program which calculates non-steady flow and transport phenomena that result from tidal and meteorological forcing on structured and unstructured, boundary fitted grids. D-Flow FM solves the shallow-water equations with the spatial discretization being achieved by a staggered finite volume method on an unstructured mesh of cells of varying complexity (Kernkamp et al., 2011).

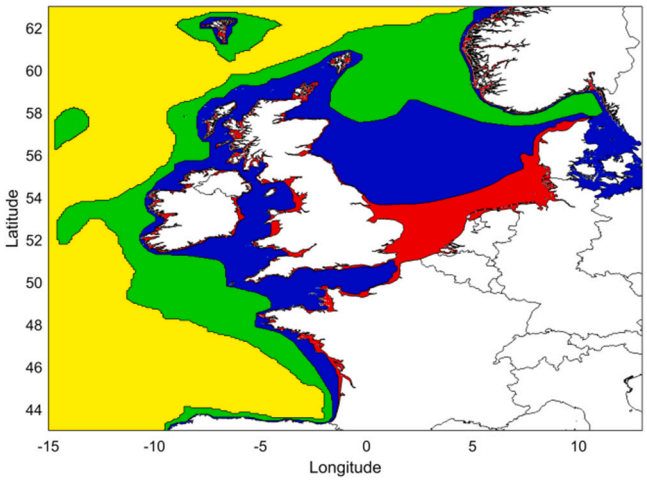


Fig. 2. Overview of the DCSM-FM model network with the colours indicating the grid size (yellow: 4 nm; green: 2 nm; blue: 1 nm; red: 0.5 nm).

The model network of 3D DCSM-FM shown in Fig. 2 covers the northwest European continental shelf, specifically the area between 15° W to 13° E and 43° N to 64° N. It has approximately 630,000 cells with a variable resolution. The largest cells (shown in yellow) have a size of 1/10° in east–west direction and 1/15° in north–south direction, which corresponds to about 4 x 4 nautical miles (nm) or 4.9–8.1 km by 7.4 km, depending on the latitude. The smallest cells (shown in red) have a size of 2/3' in east–west direction and 1/2' in north–south direction. This corresponds to about 0.5 nm x 0.5 nm or 840 m x 930 m in the vicinity of the Dutch waters. The network is specified in geographical coordinates (WGS84).

For the 3D DCSM-FM model the sigma-layer approach is used for the vertical schematization. This implies that the water column is divided into a fixed number of layers, independent of the local water depth. Consequently, the vertical resolution increases in shallow areas and changes because of water level variations in both space and time. A total of 20 layers with a uniform thickness of 5% of the local water depth is applied. This is expected to be sufficient for relatively shallow coastal areas.

For meteorological surface forcing of the model time- and space-varying wind speed (at 10 m height) and air pressure (at MSL) are derived from Hirlam7.2 (used for the simulations covering the period 2013–2017) or ECMWF ERA-Interim (used for simulations covering the period 2006–2015). The impact of the water velocity on the wind stress at the surface is taken into account in the 3D DCSM-FM model.

Spatial differences in water temperature, both horizontally and vertically, affect the transport of water through the impact it has on water density. Vertical temperature differences occur for example in the central North Sea, which is seasonally stratified due to heating of the water surface in summer. Furthermore, water temperature in shallow waters such as the Wadden Sea reacts faster to changes in meteorological conditions. This causes horizontal temperature gradients (and consequently density gradients) which under the right conditions can generate a surface flow towards deeper water and a bottom flow in opposite direction and this will affect sand transports when these flow are used as an input to a sand transport model. Therefore, transport of temperature is modelled. An important driver is the exchange of heat with the atmosphere. Therefore, a surface heat flux model is used to compute the time-and space varying exchange of heat through the air–water interface. This model requires temporally varying data on air temperature at 2 m height, cloud cover, dew point temperature and wind speed. The incoming solar radiation is then computed by the heat flux model using the latitude on earth and the position of the earth relative to the sun based on the Julian day. The net solar radiation

is computed by correcting for the cloud cover. The data sources for forcing the heat-flux model are the same as used for the wind forcing.

Rivers release significant amounts of freshwater into the North Sea. Upon entering the open sea this buoyancy input turns anti-cyclonically under the influence of the rotation of the Earth and establishes a plume downstream. Simpson (1993) introduced the name ROFI (region of freshwater influence) for such river plume areas. In the ROFI the buoyancy input competes with wind and tidal mixing to establish stratification. Tidal current profiles are significantly affected by this stratification, as well as residual current profiles (De Boer, 2009). The most important fresh water discharge in Dutch coastal waters is that of the river Rhine. The Rhine water debouches in Hoek van Holland and during periods of high discharge a fraction at sluices 15 km south (Haringvlietsluizen). The ROFI generally extends 20–40 km from the coast, with an occasional outburst 50 km offshore. The ROFI stretches alongshore to Den Helder. Here it joins with any fresh water that might come through the Texel inlet, which is significantly less than the Rhine discharge. The tidal and residual currents in the Rhine ROFI vary on two time scales, namely fortnightly and semi-diurnal with stratification being the most important parameter. Whereas the cross-shore tidal velocities are zero in the well-mixed state, during periods of stratification a significant cross shore velocity difference up to 70 cm/s emerges over the vertical (De Boer, 2009). This also affects the sand transport rates when these flows are used as an input for a sand transport model.

Fresh water discharges in the model domain are prescribed as climatological monthly means based on E-HYPE data for the years 1989–2013 (Donnelly et al., 2009, 2016). This also holds for the water temperature associated with these discharges, while the salinity is set to a constant value of 0.001 psu, reflecting fresh water conditions. All discharges are prescribed in a depth averaged fashion.

Of the 895 E-HYPE based discharges imposed throughout the model domain, the six most important ones in the Netherlands are replaced by the actual discharges as available from Rijkswaterstaat (https://waterinfo.rws.nl/), i.e. Den Oever Buiten, Haringvlietsluizen Binnen, IJmuiden Binnen, Kornwerderzand Buiten, Maassluis and Schaar van Oude Doel. Since associated water temperatures are not available, these are set to a constant of 11 °C.

2.2. Wave transformation matrix

The necessary wave parameters to compute the sand transports are taken from wave observation data in combination with a wave transformation matrix or wave look-up table to assess the wave conditions anywhere along the Dutch coast. The wave transformation matrix is described by De Fockert and Luijendijk (2011). The wave transformation matrix enables a swift transformation of measured offshore wave time series from the Schouwenbank, Lichteiland Goeree, IJmuiden, Europlatform, Eierlandse Gat and Schiermonnikoog wave buoys to an arbitrary location nearshore.

The wave transformation matrix was made by analysing the offshore wave observation data and classifying these into discrete wave height, wave period and wave direction bins. These offshore wave conditions were applied to drive SWAN wave models (Booij et al., 1996, 1999; Ris et al., 1999) of different parts of the Dutch coast. A set of 269 stationary SWAN computations were made to obtain good insight in the wave transformation under different hydrodynamic conditions.

A wave transformation matrix was made using the offshore wave conditions and the generated nearshore wave conditions. For the significant wave height and peak period, the transformation matrix was filled with multiplication factors and for the wave direction and surge an additional factor was applied.

In the wave transformation matrix, nearshore wave conditions depend more strongly on wave observation data that are closest by. For example, along the Holland coast, waves that have a direction smaller than 280° use the offshore wave information of Europlatform and waves with a direction larger than 280° use the wave information of IJmuiden. For the region above IJmuiden, waves with a direction smaller than 300° use the offshore wave information of IJmuiden and waves with a direction larger than 300° use the wave information of Eierlandse Gat as offshore wave platform. The wave transformation matrix uses wave height (Hm0), wave spectrum peak period (Tp), wave direction (Θ), wind speed, wind direction and surge.

2.3. Transport module

The flow and wave parameters feed into a local 1DV sand transport model. It is assumed that the sediment concentrations in the water column are determined by local conditions, which is a valid approach if sandy sediment is considered. We apply an extended version of the 1DV sediment transport model by Van Rijn et al. (2018). It is an engineering approach of the model by Van Rijn (2007a,b) and described in more detail by Grasmeijer (2018). Wave-driven flow effects are excluded or accounted for in a simplified way.

The suspended sand transport is computed by integration of the product of velocity and concentration over the water depth:

$$q_s = \sum_{a}^{h} (uc)\, dz$$

with a the reference height above the bed, h the water depth, and u and c the velocity and concentration at height z above the bed. The grid points over the depth (50 points) are distributed with most points close to the bed and an exponential distribution towards the water surface.

The bedload sand transport includes the effect of wave skewness and computes the bedload transport based on the quasi-steady approach by Van Rijn (2007a) as follows:

$$q_b = \int_{o}^{T} q_{b,t} dt$$

with $q_{b,t}$ the intra-wave time-dependent bedload transport and T the wave period. For the quasi-steady bedload transport approach, the intra-wave near-bed velocity is computed based on the parameterization by Isobe and Horikawa (1982).

The total load transport of sand is computed as the sum of the suspended load and bed load.

3. Model validation

The 3D DCSM-FM water levels have been validated for 13 stations along the Dutch coast, sea surface salinities for 11 stations and velocities for 4 stations. The output of the wave transformation matrix has been validated for two wave buoys along the Holland coast. Fig. 3 shows the locations of the measurement stations used for model validation.

3.1. 3D DCSM-FM: water levels

Table 1 presents the quality of the water level representation of the 3D DCSM-FM model for the calendar years 2013–2015 in terms of the Root-Mean-Square Error (RMSE) for a selection of 13 stations along the Dutch coast, considering tide, surge, total water level (Zijl et al., 2018). The tidal and surge part of the total water level were derived by harmonic analysis using t_tide and prescribing a set of 118 constituents. The average total water level RMSE is 9–10 cm. The contribution of the tide to the total water level error was larger than the contribution of the surge. On the whole, the 3D DCSM-FM model represents the water levels very accurately.

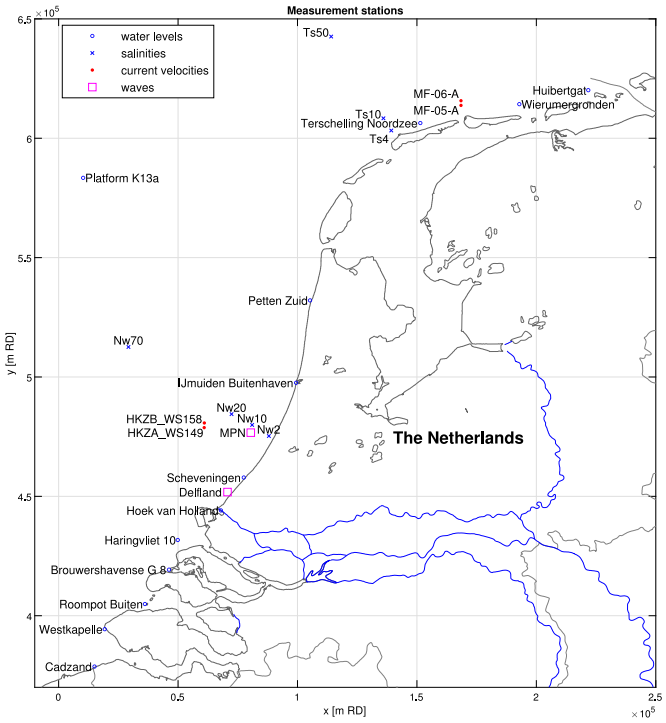


Fig. 3. Measurement stations used for 3D DCSM-FM model validation.

Table 1
Water level representation (RMSE, determined for the years 2013–2015) 3D DCSM-FM, at 13 locations along the Dutch coast, for tide, surge and total water level signal. See Fig. 3 for locations.

Station	RMSE tide (cm)	RMSE surge (cm)	RMSE water level (cm)
Cadzand	7.3	5.5	9.2
Westkapelle	8.3	5.4	9.9
Roompot Buiten	9.6	5.5	11.1
Brouwershavense G 8	6.9	6.4	9.2
Haringvliet 10	7.8	5.8	9.7
Hoek van Holland	9.9	6.4	11.8
Scheveningen	8.0	6.0	10.0
IJmuiden Buitenhaven	7.8	6.1	9.9
Petten Zuid	9.0	7.3	11.6
Platform K13a	6.7	4.3	8.0
Terschelling Noordzee	6.4	5.6	8.5
Wierumergronden	6.3	5.3	8.2
Huibertgat	6.6	5.6	8.6
Average	7.8	5.8	9.7
RMS	7.8	5.8	9.7

3.2. 3D DCSM-FM: sea surface salinity

Fig. 4 shows the computed sea surface salinity on 22-03-2006 (left) and 21-04-2006 (right) illustrating the temporal and spatial variability. The salinity in the Rhine Region Of Freshwater Influence (De Boer, 2009), a complex three-dimensional body of low salinity water in the North Sea, is much more variable than the interval with which measurements are available. Therefore, we compared the computed sea surface salinity to measurements along two cross-shore transects for the ten-year period 2006 to 2015. Fig. 3 shows the locations Nw2, Nw10, N20 and Nw70 along the Noordwijk transect and Ts4, Ts4 and Ts50 along the Terschelling transect. A quantitative assessment of the sea surface salinity representation is presented in Table 2 for the Noordwijk transect and in Table 3 for the Terschelling transect. The observed average salinity in the Noordwijk transect varies from about 29 psu at Nw2 to 35 psu at Nw70 while in the Terschelling transect it varies from

Table 2
Overview of the quality of the sea surface salinity representation in the 3D DCSM-FM model at the Noordwijk transect, in terms of bias, standard deviation (std) and Root-Mean-Square Error RMSE. See Fig. 3 for locations.

Station	Bias (psu)	Std (psu)	RMSE (psu)
Noordwijk 2 km (Nw2)	0.9	1.4	1.6
Noordwijk 10 km (Nw10)	0.5	1.2	1.2
Noordwijk 20 km (Nw20)	0.8	1.2	1.4
Noordwijk 70 km (Nw70)	0.2	0.3	0.4
Average	0.6	1.0	1.2

Table 3
Overview of the quality of the sea surface salinity representation in the 3D DCSM-FM model at the Terschelling transect, in terms of bias, standard deviation (std) and Root-Mean-Square Error RMSE. See Fig. 3 for locations.

Station	Bias (psu)	Std (psu)	RMSE (psu)
Terschelling 4 km (Ts4)	0.5	1.2	1.3
Terschelling 10 km (Ts10)	0.6	0.8	1.0
Terschelling 50 km (Ts50)	0.6	0.5	0.8
Terschelling 100 km (Ts100)	0.6	0.3	0.6
Terschelling 135 km (Ts135)	0.6	0.3	0.6
Terschelling 175 km (Ts175)	0.4	0.2	0.5
Terschelling 235 km (Ts235)	0.3	0.3	0.4
Average	0.5	0.5	0.8

32 psu at Ts4 to 34.5 psu at Ts50 (Zijl et al., 2018). The average model bias is 0.6 psu for Noordwijk and 0.5 psu for Terschelling. The average standard deviation is 1.0 and 0.5 respectively and the average RMSE 1.2 and 0.8 psu. This means that the 3D DCSM-FM model represents the sea surface salinity with sufficient accuracy to simulate density driven currents and resulting mean residual flows.

3.3. 3D DCSM-FM: velocity

Two datasets have been used to validate the 3D DCSM-FM velocities. The first is from two buoys deployed by Fugro (HKZA_WS149 and HKZB_WS158) located 27 to 28 km offshore from the Egmond coast, where the water depth is approximately 23 m. Both buoys collected velocity data at 9 vertical locations, between 4 m and 20 m below the water surface, with an interval of 2 m. The data collection started in June 2016, but the data from HKZA_WS149 is only available from November 2016. The data is available until December 2017. Table 4 shows the performance statistics. The model accurately predicts the depth-averaged flow velocities, reflected by the high correlation coefficient R of 0.95 to 0.96. The model slightly overestimates the velocity magnitudes, indicated with positive values for the bias of 0.06 m/s.

The second dataset is from the Coastal Genesis 2.0 measurement campaign (Van Prooijen et al., 2020). Here we use the data from two equipped frames placed on the seabed just offshore of the ebb tidal delta of the Ameland inlet in 18 m to 20 m of water depth . The current velocity data were collected with Acoustic Doppler Current Profilers (ADCPs), measuring from 3 m to 4 m from the bed towards the water surface, with an interval of 0.8 m. The measurements were collected in different periods of 2 to 4 weeks in November and December 2017. Table 5 presents the model performance statistics for two selected stations, i.e. MF-05-A and MF-05-A. With a correlation coefficient R of 0.86–0.92, the depth-averaged velocity magnitude agrees reasonably with the measurements at these locations. The bias amounts to −0.01 to −0.03 m/s, which means that the velocities are slightly underestimated. Fig. 5 plots modelled and measured time-averaged flow velocity profiles for MF-05-A and MF-060 A for the period November–December 2017, showing that the model reasonably predicts the velocity variation over depth. This figure also illustrates slight underestimation of the velocities at MF-05-A.

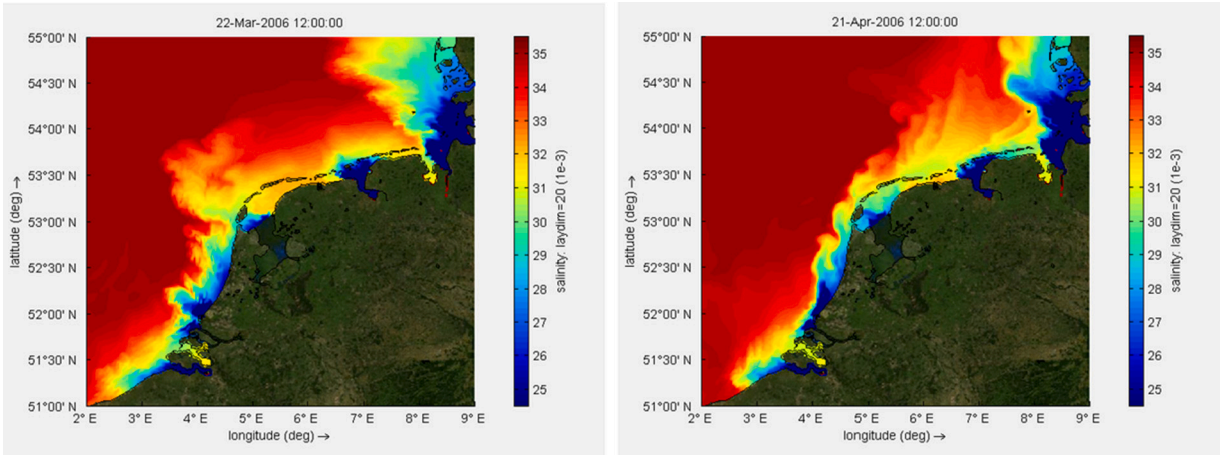


Fig. 4. Sea surface salinity on 22-03-2006 (left) and 21-04-2006 (right) as computed with 3D DCSM-FM.

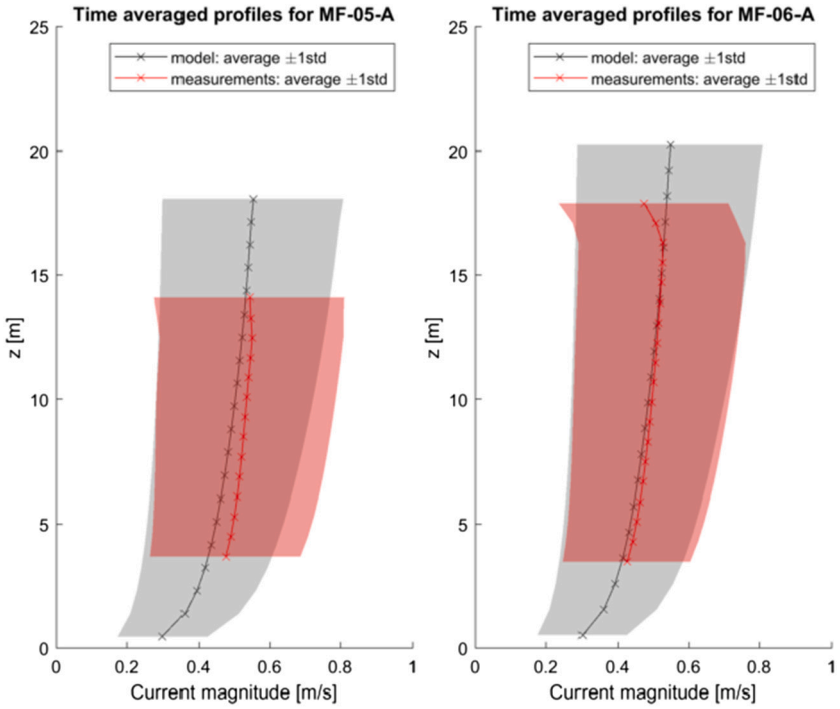


Fig. 5. Modelled (grey) and measured (red) time-averaged flow velocity profile at station MF-05-A (left) and MF-06-A (right) for the period November to December 2017. See Fig. 3 for locations. (For interpretation of the references to colour in this figure legend, the reader is referred to the web version of this article.)

Table 4
Summary of statistics of velocity data-model comparison for stations HKZA (November 2016 to December 2017) and HKZB (June 2016 to December 2017). See Fig. 3 for locations.

Station	R (–)	Bias (m/s)	Std (m/s)	RMSE (m/s)
HKZA	0.95	0.06	0.06	0.09
HKZB	0.96	0.06	0.06	0.08

3.4. Wave transformation matrix

We validated the output of the wave transformation matrix for two wave buoys along the Holland coast, i.e. Meetpost Noordwijk (MPN) and Delfland. Fig. 3 shows the wave buoy locations. Fig. 6 shows an example of observed and hindcasted significant wave height and wave spectrum peak period time series for station MPN and Fig. 7 that for station Delfland ZM01. The significant wave heights from the wave transformation matrix agree well with the observations with an RSME of 0.10 m and 0.21 m for MPN and Delfland, respectively. For the wave spectrum peak period the RMSE is 0.57 s and 0.86 s for these stations.

4. Results

As the sand transports are influenced by mean residual flows, tidal flows and waves, we will firstly discuss these hydrodynamic parameters and thereafter discuss their effect on the net annual sand transport rates. We present flow and wave parameters and computed transports at different locations along the present offshore boundary of the coastal foundation at NAP-20 m and the cross-shore variation of the transports in two different cross-shore transects. Fig. 8 shows the transects and contour line.

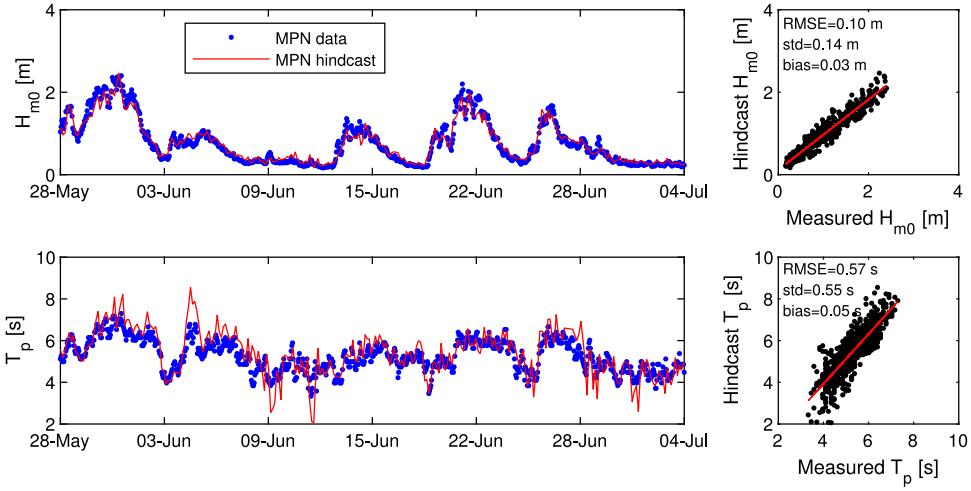


Fig. 6. Example of observed and hindcasted significant wave height and wave spectrum peak period for station MPN. See Fig. 3 for locations.

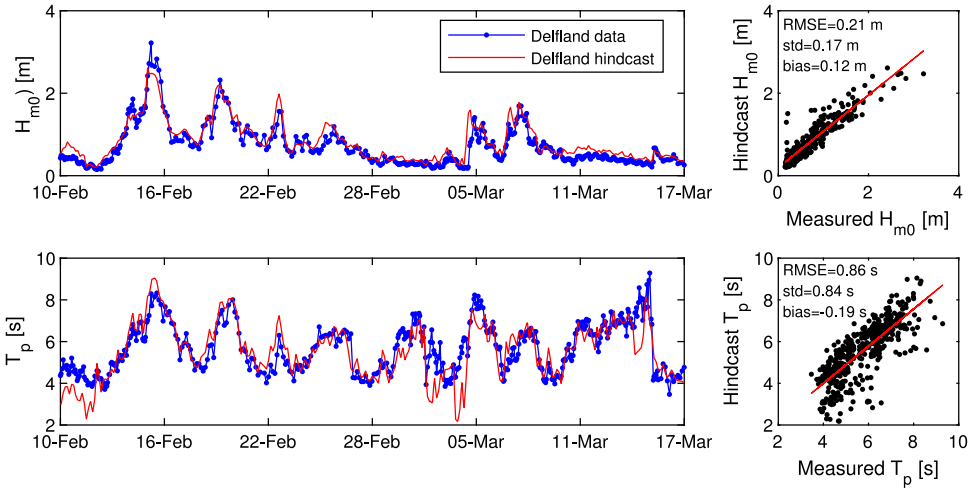


Fig. 7. Example of observed and hindcasted significant wave height and wave spectrum peak period for station Delfland. See Fig. 3 for locations.

Table 5
Summary of statistics of velocity data-model comparison for stations MF-05-A and MF-06-A for the period November to December 2017. See Fig. 3 for locations.

Station	R (–)	bias (m/s)	Std (m/s)	RMSE (m/s)
MF-05-A	0.86	−0.03	0.12	0.12
MF-06-A	0.92	−0.01	0.08	0.08

4.1. Flow velocities

4.1.1. Annual mean residual flow

Mean residual flows affect the annual mean transport rates. For example, onshore directed near-bed currents are generated by density gradients affecting onshore directed transport rates (e.g. Van Rijn, 1997). The effect of these density currents varies along the coast. Offshore directed near-bed velocities and resulting offshore transport may be generated by onshore directed winds (e.g. Héquette and Hill, 1993). To illustrate the variation of annual mean flows along the Dutch coast, we present the computed annual mean residual flows near the bed, near the surface and depth-averaged values at nine locations along the offshore boundary of the Dutch coastal foundation at NAP-20 m based on computations with the 3D DCSM-FM model for the years 2013–2017 (Fig. 9).

The computed annual mean residual flows offshore between Westkapelle and Callantsoog (Zeeland and Holland coast) show a clear effect of the wind and of the fresh water outflow of the river Rhine and the Haringvliet into the saline North Sea. This causes a difference in magnitude and direction between the near-bed and near-surface flows. The near-bed velocities are more shoreward directed and the near-surface flows more alongshore directed and sometimes have a clear offshore directed component. The near-surface flows are larger at Hoek van Holland because of the River Rhine outflow and flow contraction due to the presence of Maasvlakte II (MVII, reclaimed land near Hoek van Holland).

Computed depth-averaged annual mean residual flow magnitudes are relatively small along the Zeeland coast at Westkapelle and Oudorp (0.01 m/s), increase to 0.03–0.04 m/s along the Holland coast at Scheveningen and IJmuiden and increase further to 0.06–0.08 m/s at Callantsoog and Texel. The mean residual flow decreases to 0.03–0.04 m/s at Terschelling and Schiermonnikoog. The residual flows near the bed are smaller and generally have an onshore directed component. This onshore component is less pronounced at Callantsoog and Texel.

As sand concentrations are largest near the bed, the near-bed velocities are important for the direction of the transports. Fig. 10 shows the annual mean residual near-bed flows along the offshore boundary of the coastal foundation. The flow is now decomposed into an alongshore and a cross-shore component. This figure shows that the alongshore directed residual near-bed flows are small between Westkapelle and Scheveningen and increase to about 0.05 m/s at the height of the tidal inlet between Callantsoog and Texel (Marsdiep). The alongshore

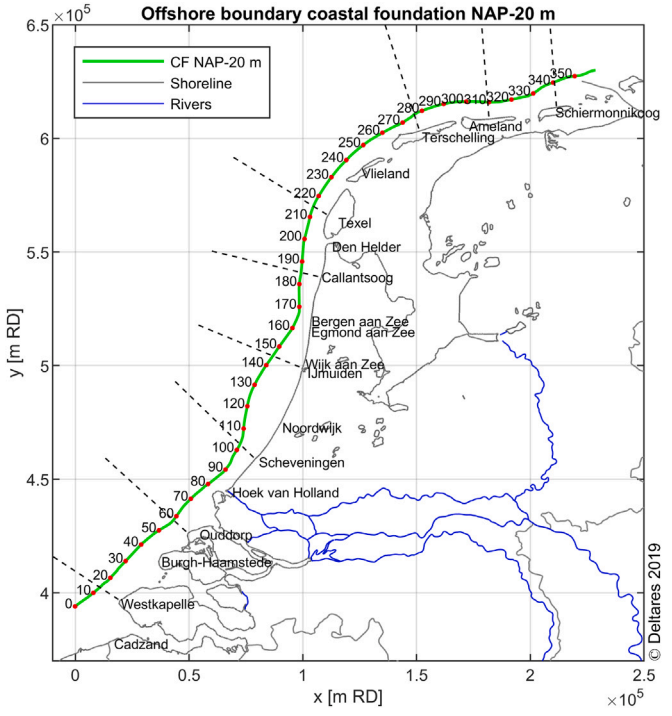


Fig. 8. Offshore boundary of the coastal foundation at NAP-20 m. The dashed lines indicate the JARKUS transects at which the flow and wave parameters and computed transports are presented in this paper.

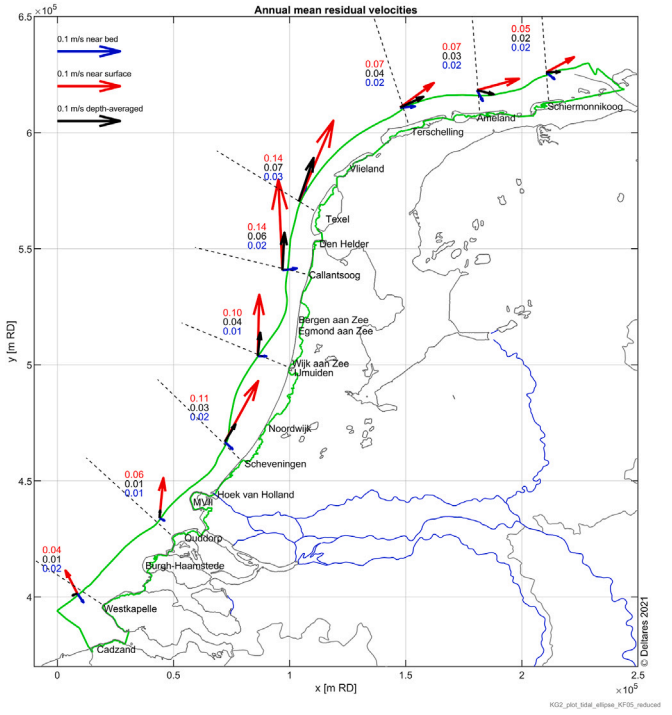


Fig. 9. Annual mean residual flows along the offshore boundary of the coastal foundation at NAP-20 m based on velocities computed with 3D DCSM-FM model. The boundary of the coastal foundation is indicated by the green polygon.

directed residual near-bed flow reduces again to about 0.02 m/s at Schiermonnikoog. The cross-shore directed residual near-bed flows are largest between Ouddorp and Scheveningen with onshore directed values of about 0.03 m/s and reduce to negligibly small values just south

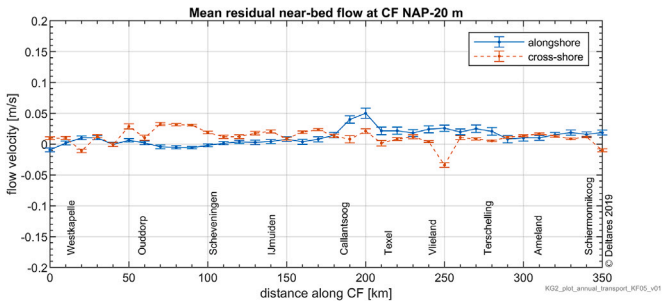


Fig. 10. Annual mean residual near-bed flows along the offshore boundary of the coastal foundation at NAP-20 m contour based on velocities computed with 3D DCSM-FM model.

of Texel. Offshore directed residual near-bed flows (about −0.03 m/s) are present at the height of the inlet between Vlieland and Terschelling (Vliestroom). The near-bed residual flow is onshore directed between Terschelling and Schiermonnikoog with values of about 0.01 m/s.

4.1.2. Peak tidal velocities

As the tidal wave propagates from south to north along the Dutch coast it becomes increasingly distorted with shorter tidal rise than tidal fall. This is most pronounced along the Holland coast and results in stronger flood currents than ebb currents (asymmetry in tidal currents). To assess the variation of the tidal velocities along and across the coast, we computed the mean of all peak flood and ebb velocities from the 3D DCSM-FM model results in a year. Fig. 11 plots the annual mean peak flood and ebb velocities as vector plots for nine different locations along the Dutch coast. To illustrate the variation in peak tidal velocities along the Dutch coast, Fig. 12 shows the annual mean peak flood and ebb velocities along the present Dutch coastal foundation (continuous NAP-20 m line). This figure shows that the peak flood velocities are larger than the peak ebb velocities along the entire Dutch coast, with a tidal velocity asymmetry larger than 0.5. There is no clear trend between Westkapelle and Ouddorp. The peak ebb velocities decrease slightly between Ouddorp and Scheveningen, where the peak flood velocities remain more or less the same. This results in an increase in the tidal velocity asymmetry along this line. The peak tidal velocities decrease slightly between Scheveningen and IJmuiden and the tidal velocity asymmetry stays more or less constant. The peak flood velocities increase between IJmuiden and Callantsoog where the peak ebb velocities remain the same, which results in an increase of the tidal velocity asymmetry here. Largest peak flood velocities at the NAP-20 m contour occur at the height of the tidal inlet between Callantsoog and Texel and also the large tidal velocity asymmetry occurs here. The annual mean peak flood velocities decrease between Texel and Terschelling where the peak ebb velocities remain the same. This results in a decrease of the tidal velocity asymmetry. Both the peak flood and ebb velocities decrease further from Terschelling to Ameland. The tidal velocity asymmetry stays more or less the same here. Alongshore variations between Ameland and Schiermonnikoog are small.

4.2. Waves

The frequency of occurrence of waves along the Holland coast is highest for waves from WSW and WNW. Waves are also highest from these directions (e.g. Roskam, 1988). North of Schiermonnikoog, the dominant direction is WNW to NNW. Fig. 13 illustrates this by showing the wave roses for eight different locations along the Dutch coast based on the years 2013–2017 as obtained from the wave transformation tool. Annual mean significant wave heights (black numbers), the 90% exceedance values (blue numbers) and the maximum significant wave heights (black numbers) are also given. This figure shows that waves

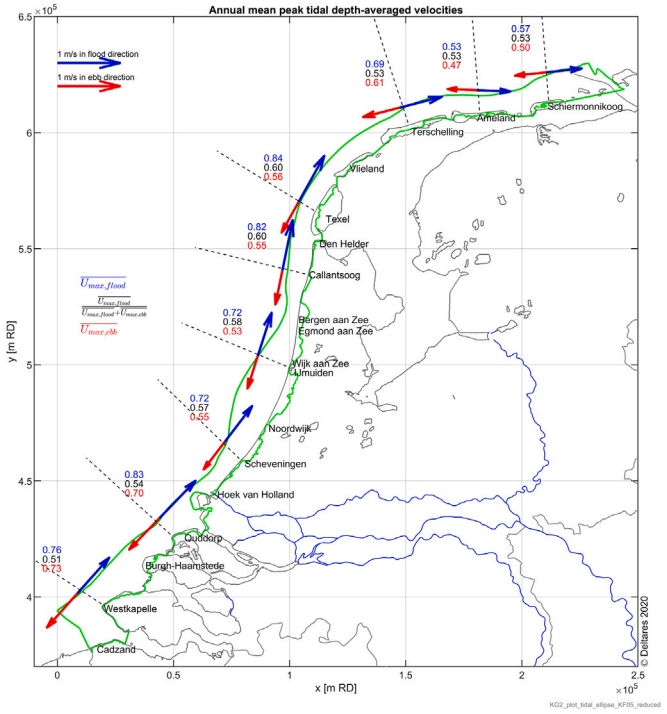


Fig. 11. Annual mean peak tidal velocities along the offshore boundary of the coastal foundation at NAP-20 m based on velocities computed with 3D DCSM-FM model.

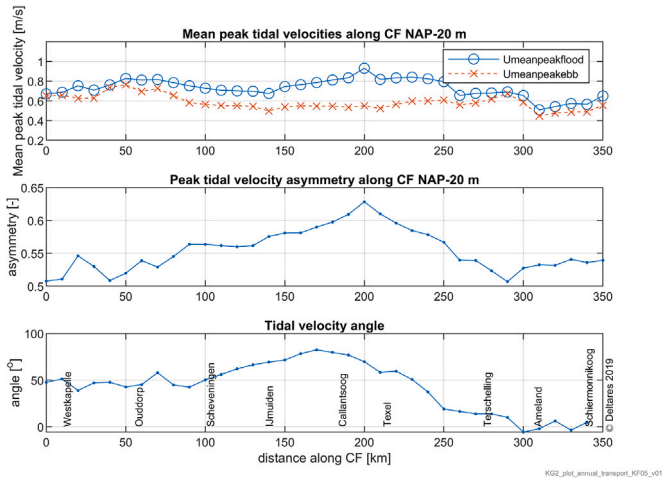


Fig. 12. Mean peak tidal velocities along the offshore boundary of the coastal foundation at NAP-20 m based on velocities computed with 3D DCSM-FM model.

are generally higher along the northern part of the Dutch coast as compared to the southern and central part.

Annual mean significant wave height $H_{m0,mean}$ at the offshore boundary of the coastal foundation is just over 1 m at Westkapelle, Ouddorp and Scheveningen. It increases to about 1.2 m at IJmuiden and Callantsoog and is about 1.3 m at Texel. The annual mean significant wave height is about 1.2 m at Terschelling and Schiermonnikoog.

The average 90% exceedance value $H_{m0,90\%}$ ranges between 1.9 and 2.3 m along the Dutch coast, with highest values offshore Texel. The maximum significant wave height $H_{m0,max}$ is 5.1–5.6 m at Westkapelle, Ouddorp and Scheveningen. It increases to about 6.1–6.5 m at Callantsoog, Texel and Terschelling. The $H_{m0,max}$ is 7.2 m at Schiermonnikoog. The maximum wave height varies from year to year with about 0.4–1.2 m.

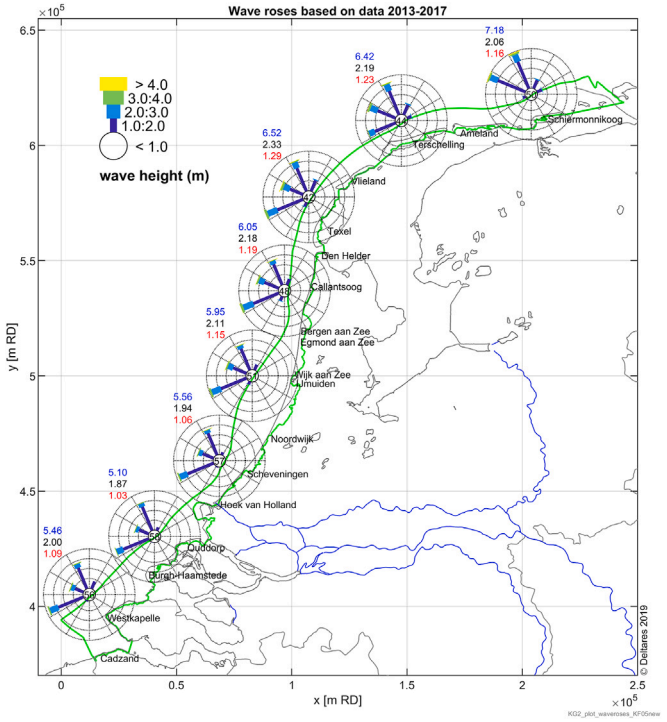


Fig. 13. Wave roses at eight locations along the Dutch coast based on the years 2013–2017. Red numbers indicate the mean significant wave height, black numbers the 90% exceedance value and blue numbers the maximum significant wave height. The numbers in the middle of the wave roses indicate the percentage $H_{m0} < 1$ m. (For interpretation of the references to colour in this figure legend, the reader is referred to the web version of this article.)

The average annual mean wave spectrum peak period Tp varies between 5.3 and 5.7 s with longest wave periods at Callantsoog, Texel and Terschelling (not shown).

4.3. Sand transports

4.3.1. Annual transports

Fig. 14 shows the computed annual mean transports as vectors along the offshore boundary of the coastal foundation (continuous NAP-20 m line). The transport rate decreases from Westkapelle to Scheveningen and increases again towards Callantsoog and Texel. Annual mean transports become much smaller towards Terschelling, Ameland and Schiermonnikoog. At most locations the transport vector tends to have an onshore component and at some an offshore component. To quantify the net effect, we decomposed the transport rates into cross-shore and alongshore component using the offshore boundary of the coastal foundation as a coast angle and determined the cross-shore transports for 19 different compartments along the Dutch coast with the continuous NAP-20 m line as an offshore boundary. Fig. 15 shows the resulting annual mean cross-shore transports. The annual mean cross-shore transports are onshore directed for most coastal compartments. The total cross-shore transport over the entire contour line is 3.6 million m^3/year. The effect of storms can be partly derived from the standard deviation of the transports over the five calculated years. This standard deviation is 0.9 million m^3/year. This means that the total cross-shore transport can be 3.6 million m^3/year one year, 2.7 million m^3/year the next and 4.5 million m^3/year the following year, depending on the storminess of the year in question.

In addition to the computations over the continuous NAP-20 m line, we made computations using the continuous NAP-18 and NAP -16 m lines as an offshore boundary and sensitivity computations to investigate the effect of return flow and grain size (Table 6). The annual

Table 6
Calculated total net annual cross-shore sand transport and standard deviation in m^3/year in landward direction over the 20 m, 18 m and 16 m depth contours along the Dutch coast. See text for model details.

Model setting	NAP-20 m	NAP-18 m	NAP-16 m
1. D_{50} = 250 μm, no return flow	3.6 ± 0.9	5.0 ± 1.4	7.1 ± 2.0
2. D_{50} = 250 μm, return flow	3.0 ± 0.8	4.3 ± 1.2	6.4 ± 1.9
3. D_{50} = 275 μm, no return flow	3.5 ± 1.0	4.9 ± 1.4	7.1 ± 2.1

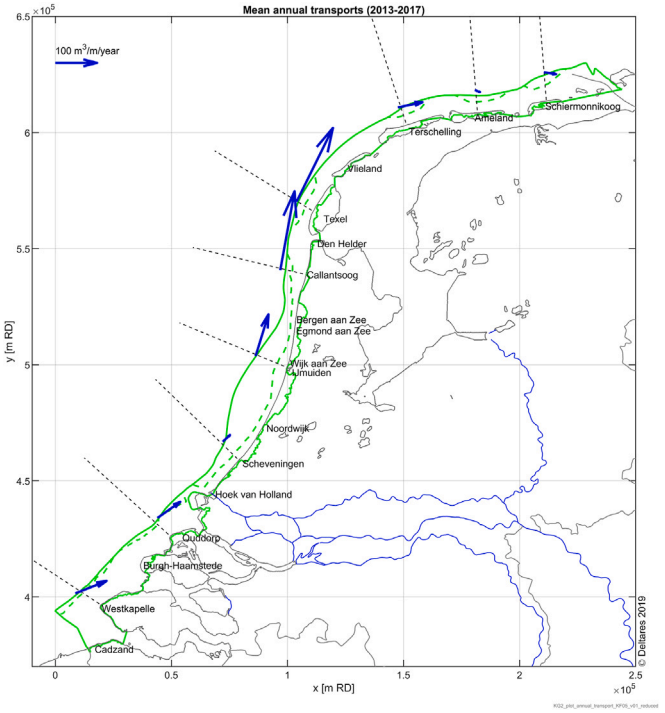


Fig. 14. Annual mean sand transports at nine locations along the Dutch coast.

mean cross-shore transport is onshore directed over all three depth contours and increases with decreasing water depth due to increased sediment stirring by waves. Including the effect of return flow reduces the transports by 11%–18%. Using a 10% larger grain size reduces the transports by 1%–10%. Note that these transports do not include the potentially large effects of very large (NW) storms that did not occur in the modelled 2013–2017 period.

To illustrate the cross-shore variation of the transports, we selected two cross-shore transects on the Dutch coast, i.e. at Scheveningen and Callantsoog. Fig. 16 shows the computed annual mean cross-shore and alongshore transports along the Scheveningen transect for model setting 1 (D_{50} = 250 μm, no return flow). The alongshore transports are about 25 m^3/m/year at 6 km (17 m depth) and decrease to 20 m^3/m/year at 10 km (20 m depth). The alongshore transports increase again to 30 m^3/m/year at 25 km (23 m depth). The computed cross-shore transports are about 5 m^3/m/year at 6 km (17 m depth) and decrease to 3 m^3/m/year at 10 km (20 m depth). The computed cross-shore transports are negligibly small at 25 km offshore (23 m depth).

Fig. 17 shows annual mean transports in the Callantsoog transect. The alongshore transport is about 190 m^3/m/year at 6 km (15 m depth). This increases slightly to 225 m^3/m/year at 8 km (20 m depth) and decreases to 210 m^3/m/year at 25 km (25 m depth).

The annual mean cross-shore transport in the Callantsoog transect is −12 m^3/m/year at 6 km (15 m depth) and about −20 m^3/m/year at 8 km (20 m depth). At 25 km (23 m depth) this is −13 m^3/m/year.

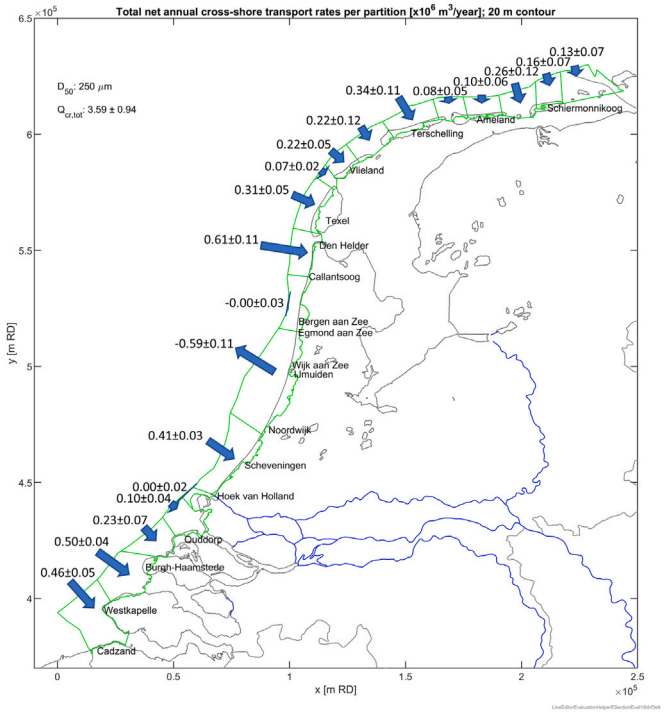


Fig. 15. Cross-shore sand transports per partition.

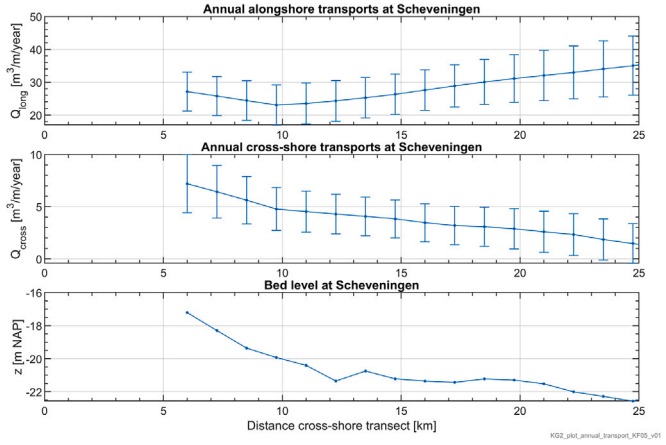


Fig. 16. Computed net annual mean cross-shore and alongshore transports along two transect (see Fig. 8. Statistics are based on annual means over years 2013–2017 and error bars indicate the standard deviation between the years. The lower panel shows the bed levels along this transect.

4.3.2. *Effect of density and wind*

We studied the effect of density and wind on the annual mean transport rates and directions by making transport computations with density switched off and with both density and wind switched off in the 3D DCSM-FM model. Both scenario's included waves from the wave transformation matrix. This is a theoretical exercise of course as in reality density effects will always be present due to fresh water outflow of the Rhine into the North Sea for example, and without wind no waves would be generated in reality. But it gives an impression of the relative effects of density and wind on the transport rates. We illustrate the effect of density and wind for the Scheveningen and Callantsoog transects.

In the Scheveningen transect, switching off the effects of density leads to about 40% larger alongshore transports and 100% reduction of onshore directed cross-shore transports or a change to offshore

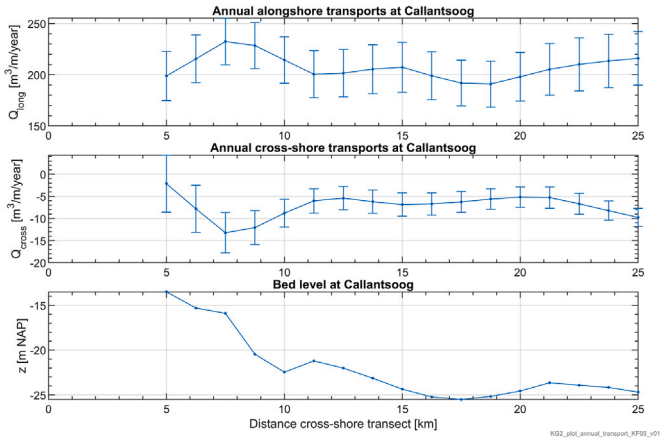


Fig. 17. Computed net annual mean cross-shore and alongshore transports along two transect (see Fig. 8). Statistics are based on annual means over years 2013–2017 and error bars indicate the standard deviation between the years. The lower panel shows the bed levels along this transect.

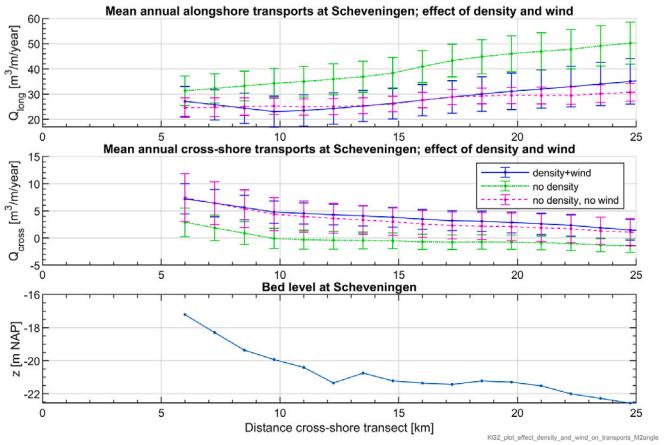


Fig. 18. Computed annual mean cross-shore and alongshore transports along the Scheveningen transect (see Fig. 8). Error bars indicate the standard deviation between the years 2013–2017. The lower panel shows the bed levels along this transect.

direction (Fig. 18). At 20 m water depth this results in a change from about 4 m^3/m/year onshore directed transport to a negligible small value when switching off density. In addition, when we also switch off wind this effect is largely counteracted, but the cross-shore transport is still about 20% smaller compared to the situation with wind and density switched on.

In the Callantsoog transect, switching off density results in an increase of the alongshore transport by about 30% (Fig. 19). The offshore directed cross-shore transport increases with more than a factor 2. At 20 m water depth this results in a change from −12 to −24 m^3/m/year. In addition, also switching off wind counteracts this effect and results in onshore directed transports in water depths shallower than 20 m.

Although strongly schematized, the sensitivity analysis by Van Rijn (1997) showed a contribution of the fluid density effect to the cross-shore transport at a depth of 20 m of about 10 to 25 m^3/m/year (onshore directed). Our 3D computations show a contribution of the density effects of 5 to 7 m^3/m/year, which is just below the lower limit of the range estimated by Van Rijn (1997).

4.3.3. Contribution of storm events

Besides deriving the effect of a stormy or calm year from the standard deviation of the transports over the five calculated years, we

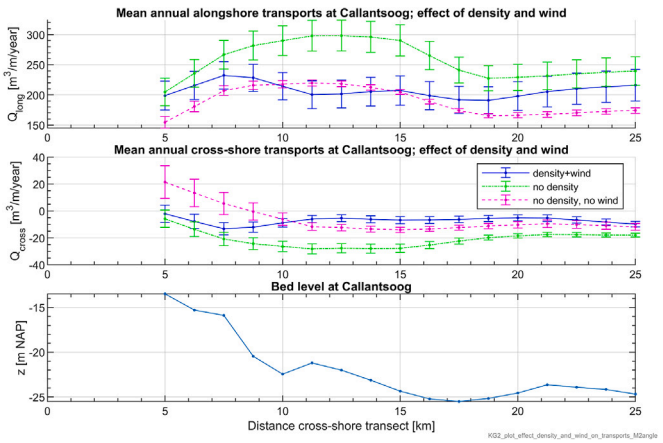


Fig. 19. Computed net annual mean cross-shore and alongshore transports along the Callantsoog transect (see Fig. 8). Error bars indicate the standard deviation between the years 2013–2017. The lower panel shows the bed levels along this transect.

studied the relative importance of different wave heights on the cross-shore transports in more detail by clustering the computed cross-shore transports into different wave height classes and by determining the relative contribution of each wave height class to the total cross-shore transport rate for the year 2013. Here we will show the analysis at 20 m water depth for two different locations, i.e. Scheveningen and Callantsoog. Fig. 20 shows the cross-shore transports as a function of wave height, the probability of different wave height classes and the relative contribution of each wave height class to the total cross-shore transport rate at Scheveningen and the contribution to on- or offshore directed transports. Fig. 21 shows the same for Callantsoog. These figures illustrate that larger transports generally occur for larger wave heights but negligibly small transports may also occur for large wave heights if the flow velocities are small. The contribution of the different wave heights depends on their probability of occurrence. Significant wave heights of 0.5–1.0 m occur most frequently at Scheveningen and Callantsoog and the probability of occurrence decreases with increasing wave height. The net cross-shore transport is sometimes determined by a delicate balance between onshore and offshore directed components. If the net cross-shore transport during normal conditions is negligibly small because onshore and offshore components are equal in magnitude, a storm may push the balance to one direction. For example, at Scheveningen in 2013, the net cross-shore transport is onshore directed when including all wave conditions. However, excluding waves higher than 3.5 m would result in a net offshore directed transport. At Callantsoog, the highest waves contribute more to the offshore directed transports. These results suggest that storm conditions play an important role for the net transport rates at the lower shoreface.

5. Discussion

We computed the annual sand transport rates at the Dutch lower shoreface using the output from a flow model and a wave transformation tool as an input for a 1DV sand transport model. We assumed that at the lower shoreface the sand transport flux is determined locally and that the interaction of flow and waves does not substantially alter the transport. The models were validated against measurements. However, with this approach we may have underestimated residual flows during high wave events, which would result in an underestimation of the transport rates under these conditions and the relative contribution of these conditions to the net annual mean transport rate. Therefore, we advice to validate this approach by making computations with a so-called online approach, including the interaction of flow and waves.

The alongshore transports in the Scheveningen transect at 20 depth of a about 20 m^3/m/year computed here are within the range of

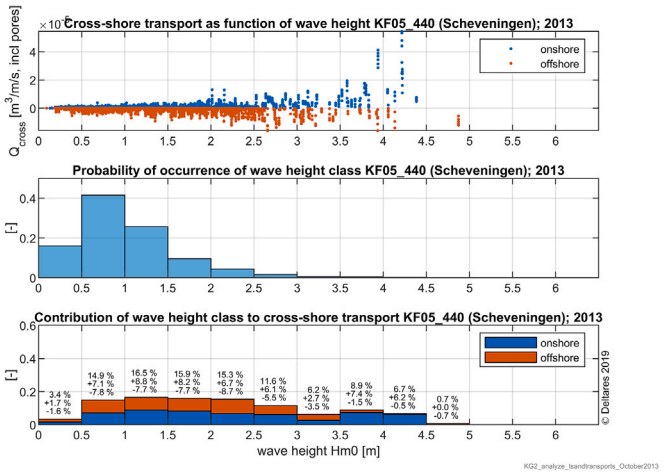


Fig. 20. Transports as a function of wave height, probability of different wave height classes and relative contribution of each wave height class to the total cross-shore transport rate at Scheveningen.

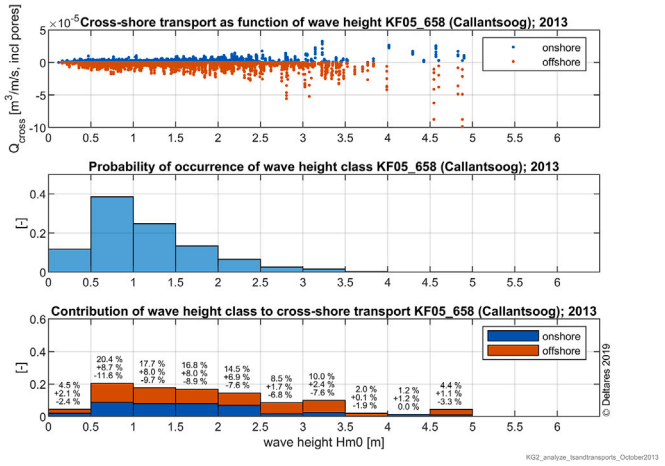


Fig. 21. Transports as a function of wave height, probability of different wave height classes and relative contribution of each wave height class to the total cross-shore transport rate at Callantsoog.

25 ± 15 m^3/m/year as computed by Van Rijn (1997) at 20 m depth. The computed cross-shore transports of about 3 m^3/m/year at 20 m depth are also within the range of 0 ± 10 m^3/m/year as computed by Van Rijn (1997) at 20 m depth. However, the annual mean alongshore transport in the Callantsoog transect of about 225 m^3/m/year at 20 m depth is about three times larger than reported by Van Rijn (1997) at 20 m depth. This difference may have been caused by a difference in methodology. Van Rijn (1997) applied schematized tide, wind and wave conditions whereas here the transports are based on brute force computations (real time series). For example, the annual mean peak tidal flood and ebb velocities based on the brute force computations used here are 0.82 m/s and 0.55 m/s, respectively, whereas the schematized flood and ebb velocities used by Van Rijn (1997) amount to 0.66 m/s and 0.50 m/s (see Van Rijn et al., 1995). This difference could already explain a factor of 2 difference in transport rates. The annual mean cross-shore transport rates of 5 ± 10 m^3/m/year at 20 m depth in the Callantsoog transect reported by Van Rijn (1997) show an onshore directed tendency, where our computations show offshore transports in this transect. At the same time, the coastal stretch just north of Callantsoog also shows onshore directed transports in our computations (Fig. 15). This illustrates the sensitivity for the exact location for which the computations are made and the definition of the coast angle. Schematization of the wind and wave conditions and the use of a different transport model by Van Rijn (1997) also plays a role in the different estimates.

Flow and transport vectors can be decomposed into an alongshore and a cross-shore component. The magnitude of the resulting alongshore and cross-shore components depends on the definition of the coast angle. Here we used the angle of the major component of the $M2$ tide as the coast angle to present the transports at one single location or in cross-shore transect. An other definition often used in the Netherlands is the angle of the so-called JARKUS transects. For the total net annual mean cross-shore transport in different compartments along the Dutch coast we used the angle of the offshore boundary of the Dutch coastal foundation. This is a robust measure independent of conditions and facilitates assessing a sand balance for different parts of the coast.

6. Conclusions

6.1. Modelling approach

This paper presented a computationally efficient approach to compute the annual sand transport rates at the Dutch lower shoreface based on the 3D Dutch Continental Shelf Model with Flexible Mesh (3D DCSM-FM) of the entire Dutch coast, a wave transformation tool and a 1DV sand transport module.

The 3D DCSM-FM water level validation for the calendar years 2013–2015 at a selection of 13 stations along the Dutch coast showed an average total water level RMSE of 9–10 cm. The contribution of the tide to the total water level error was larger than the contribution of the surge. On the whole, the 3D DCSM-FM model represented the water levels very accurately.

Comparison of the computed sea surface salinity to measurements along the Noordwijk and Terschelling transects showed an average bias of 0.6 psu and 0.5 psu, respectively. The average standard deviation was 1.0 and 0.5 respectively and the average RMSE 1.2 and 0.8 psu. This means that the 3D DCSM-FM model represents the sea surface salinity quite accurately. This is an important aspect in simulating density driven currents and resulting mean residual flows.

Two datasets were used to validate the 3D DCSM-FM velocities. The first from two buoys deployed at 27 to 28 km offshore from the Egmond coast, where the water depth is approximately 23 m. The model accurately predicted the depth-averaged flow velocities, reflected by a high correlation coefficient R of 0.95 to 0.96. The model slightly overestimated the velocity magnitudes, indicated with positive values for the bias of 0.06 m/s. The second dataset was from the Coastal Genesis 2.0 measurement campaign (Van Prooijen et al., 2020). Data from two equipped frames placed on the seabed just offshore of the ebb tidal delta of the Ameland inlet in 18 m to 20 m of water depth were used. The depth-averaged velocity magnitude agreed reasonably with the measurements at these locations, with correlation coefficients R of 0.86–0.92. The bias amounted to −0.01 to −0.03 m/s, which means that the velocities were slightly underestimated. The model reasonably predicted the velocity variation over depth.

The output of the wave transformation matrix was validated for two wave buoys along the Holland coast, i.e. Meetpost Noordwijk (MPN) en Delfland. The significant wave heights from the wave transformation matrix agreed well with the observations with an RSME of 0.10 m and 0.21 m for MPN and Delfland, respectively. For the wave spectrum peak period the RMSE was 0.57 s and 0.86 s for these stations.

6.2. Physical processes

The net annual sand transport rates along the Dutch coast are determined by peak tidal velocities (and asymmetry thereof), density driven residual flows, wind driven residual flows and waves. The effect

of density difference and wind on the 3D structure of the flow cannot be neglected along the Dutch lower shoreface.

Density driven flow shows a tendency to be onshore directed near the bed because saline sea water flows towards the coast near the bed and fresh river water spreads out into the North Sea near the surface. Wind driven flow has a strong onshore directed component near the surface because of the predominant wind directions along the Dutch coast and the shape of the coast with respect to the wind directions. The onshore wind driven flow near the surface is generally balanced by a more offshore directed wind driven component near the bed (because of mass balance, otherwise all water would pile up at the coast). The general influence of the density-driven currents is that it enhances an onshore directed transport component. This effect is strongest along the Zeeland and Holland coast. The general influence of the wind is that it enhances an offshore directed transport component. This effect plays a role along the entire Dutch coast but is less pronounced than the density effect.

6.3. Annual mean transports at the dutch lower shoreface

Our computations showed decreasing annual mean alongshore transports from Westkapelle to Scheveningen, increasing from Scheveningen to the inlet between Callantsoog and Texel (Marsdiep) and decreasing again towards Schiermonnikoog at the continuous NAP-20 contour. The total cross-shore transports over the continuous NAP-20 m, NAP-18 m and NAP -16 m lines showed onshore directed over all three depth contours. This increased with decreasing water depth due to increased sediment stirring by waves. Including the effect of return flow reduced the transports by 11%–18%. Using a 10% larger grain size reduced the transports by 1%–10%. Although very large storms did not occur in the modelled 2013–2017 period, analysis of the cross-shore transports for different wave classes at two locations showed that the net cross-shore transport is sometimes determined by a delicate balance between an onshore and offshore directed component. If the net cross-shore transport during normal conditions is negligibly small because onshore and offshore components are equal in magnitude, a storm may push the balance to one direction. Our results suggest that storm conditions play an important role for the transport rates at the lower shoreface.

Declaration of competing interest

The authors declare that they have no known competing financial interests or personal relationships that could have appeared to influence the work reported in this paper.

Acknowledgements

This paper presents results of research performed in the Coastal Genesis 2.0 project. The executive agency of the Dutch Ministry of Infrastructure and Water Management (Rijkswaterstaat) is thanked for making this research possible and for the pleasant cooperation and valuable comments and discussions on the research findings.

References

Aagaard, T., 2014. Sediment supply to beaches: Cross-shore sand transport on the lower shoreface. J. Geophys. Res.: Earth Surf. 119 (4), 913–926. http://dx.doi.org/10.1002/2013JF003041.

Aagaard, T., Davidson-Arnott, R., Greenwood, B., Nielsen, J., 2004. Sediment supply from shoreface to dunes: Linking sediment transport measurements and long-term morphological evolution. Geomorphology 60 (1–2), 205–224. http://dx.doi.org/10.1016/j.geomorph.2003.08.002.

Anthony, E.J., Aagaard, T., 2020. The lower shoreface: Morphodynamics and sediment connectivity with the upper shoreface and beach. Earth-Sci. Rev. 210 (November), 103334. http://dx.doi.org/10.1016/j.earscirev.2020.103334.

Booij, N., Holthuijsen, L., Ris, R., 1996. The SWAN wave model for shallow water. In: Proceedings of the 25th International Conference on Coastal Engineering, January 1996. pp. 668–676.

Booij, N., Ris, R.C., Holthuijsen, L.H., 1999. A third-generation wave model for coastal regions: 1. Model description and validation. J. Geophys. Res. Oceans 104 (C4), 7649–7666. http://dx.doi.org/10.1029/98JC02622.

De Boer, G.J., 2009. On the Interaction Between Tides and Stratification in the Rhine Region of Freshwater Influence (Ph.D. thesis). Delft University of Technology, Delft, The Netherlands.

De Fockert, A., Luijendijk, A., 2011. Wave look-up table: Building with Nature, Report 1002337-002-ZKS-0001. Technical Report, Deltares, Delft, Netherlands.

Donnelly, C., Andersson, J.C., Arheimer, B., 2016. Using flow signatures and catchment similarities to evaluate the E-HYPE multi-basin model across Europe. Hydrol. Sci. J. 61 (2), 255–273. http://dx.doi.org/10.1080/02626667.2015.1027710.

Donnelly, C., Dahne, J., Lindström, G., Rosberg, J., Strömqvist, J., Pers, C., Yang, W., Arheimer, B., 2009. An Evaluation of Multi-Basin Hydrological Modelling for Predictions in Ungauged Basins, Vol. 333. IAHS-AISH Publication, pp. 112–120, September.

Grasmeijer, B., 2018. Method for calculating sediment transport on the Dutch lower shoreface, Report 1220339-000-0041. Technical Report, Deltares, Delft, The Netherlands.

Grasmeijer, B., Van Rijn, L., Van der Werf, J., Zijl, F., Huisman, B., Luijendijk, A., Wilmink, R., De Looff, A., 2019. Method for calculating annual sand transports on the Dutch lower shoreface to assess the offshore boundary of the Dutch coastal foundation. In: Proceedings of the 9th International Coastal Sediments Conference. World Scientific, pp. 2136–2149. http://dx.doi.org/10.1142/9789811204487_0183.

Héquette, A., Hill, P.R., 1993. Storm-generated currents and offshore sediment transport on a sandy shoreface, Tibjak Beach, Canadian Beaufort Sea. Mar. Geol. 113 (3–4), 283–304. http://dx.doi.org/10.1016/0025-3227(93)90023-O.

Hinton, C.L., Nicholls, R.J., 2007. Shoreface morphodynamics along the Holland Coast. In, Balson, P.S. and Collins, M.B. (eds.). Coastal and Shelf Sediment Transport. (Geological Society, London, Special Publications, 274). pp. 93–101. http://dx.doi.org/10.1144/GSL.SP.2007.274.01.10.

Isobe, M., Horikawa, K., 1982. Study on water particle velocities of shoaling and breaking waves.. Coast. Eng. Japan 25, 109–123. http://dx.doi.org/10.1080/05785634.1982.11924340.

Kernkamp, H.W., Van Dam, A., Stelling, G.S., De Goede, E.D., 2011. Efficient scheme for the shallow water equations on unstructured grids with application to the Continental Shelf. Ocean Dyn. 61 (8), 1175–1188. http://dx.doi.org/10.1007/s10236-011-0423-6.

Knook, P., 2013. Sediment transport on various depth contours of the 'Holland Coast' shoreface (MSc thesis). Delft University of Technology.

Mulder, J.P., Hommes, S., Horstman, E.M., 2011. Implementation of coastal erosion management in the Netherlands. Ocean Coast. Manag. 54 (12), 888–897. http://dx.doi.org/10.1016/j.ocecoaman.2011.06.009, Concepts and Science for Coastal Erosion Management (Conscience).

Patterson, D.C., Nielsen, P., 2016. Depth, bed slope and wave climate dependence of long term average sand transport across the lower shoreface. Coast. Eng. 117, 113–125. http://dx.doi.org/10.1016/j.coastaleng.2016.07.007.

Ris, R.C., Holthuijsen, L., Booij, N., 1999. A third-generation wave model for coastal regions: 2. Verification. J. Geophys. Res. Oceans 104, 7667–7681. http://dx.doi.org/10.1029/1998JC900123.

Roelvink, J.A., Stive, M.J.F., 1991. Sand transport on the shoreface of the Holland Coast. The Dutch Coast: Paper No. 5. In: Coastal Engineering 1990. ASCE, pp. 1909–1921. http://dx.doi.org/10.1061/9780872627765.146.

Roskam, A., 1988. Golfklimaten voor de Nederlandse kust; nota GWAO-88.046. Technical Report, Rijkswaterstaat, Dienst Getijdewateren, p. 70.

Simpson, J.H., 1993. Periodic stratification in the rhine ROFI in the north sea. Oceanol. Acta 16 (1), 23–32.

Stive, M.J., de Vriend, H.J., Nicholls, R.J., Capobianco, M., 1992. Shore nourishment and the active zone: a time scale dependent view. In: Coastal Engineering 1992. ASCE, pp. 2464–2673. http://dx.doi.org/10.1061/9780872629332.188.

Van der Hout, C., Tonnon, P., De Ronde, J., 2009. Morphological effects of mega nourishment. Report 1200659-000. Technical Report, Deltares, Delft, The Netherlands.

Van der Spek, A., Elias, E., Lodder, Q., Hoogland, R., 2015. Toekomstige suppletievolumes - Eindrapport. 1208140-005-ZKS-000. Technical Report, Deltares, Delft, The Netherlands.

Van der Spek, A., Van der Werf, J., Grasmeijer, B., Schrijvershof, R., Vermaas, T., 2022. The lower shoreface of the Dutch coast - an overview. Ocean Coast. Manag. in this issue.

Van der Werf, J., Giardino, A., 2009. Effect van een zeer grooschalige zandwinning langs de nederlandse kust op de waterbeweging, zandtransporten en morfologie. Report nr. 1200996-000-ZKS-0010. Technical report, Deltares, Delft, The Netherlands, p. 74.

Van Prooijen, B.C., Tissier, M.F., De Wit, F.P., Pearson, S.G., Brakenhoff, L.B., Van der Vegt, M., Mol, J.W., Kok, F., Holzhauer, H., Van der Werf, J.J., Vermaas, T., Gawehn, M., Grasmeijer, B., Elias, E.P., Tonnon, P.K., Reniers, Ad, J., Wang, Z.B., Den Heijer, C., Van Gelder-Maas, C., Wilmink, R.J., Schipper, C.A., De Looff, H., 2020. Measurements of hydrodynamics, sediment, morphology and benthos on Ameland ebb-tidal delta and lower shoreface. Earth Syst. Sci. Data 12 (4), 2775–2786. http://dx.doi.org/10.5194/essd-12-2775-2020.

Van Rijn, L.C., 1997. Sediment transport and budget of the central coastal zone of Holland. Coast. Eng. 32 (1), 61–90. http://dx.doi.org/10.1016/S0378-3839(97)00021-5.

Van Rijn, L.C., 2007a. Unified view of sediment transport by currents and waves. I: Initiation of motion, bed roughness, and bed-load transport. J. Hydraul. Eng. 133 (6), 649–667. http://dx.doi.org/10.1061/(ASCE)0733-9429(2007)133:6(649).

Van Rijn, L.C., 2007b. Unified view of sediment transport by currents and waves. II: Suspended transport. J. Hydraul. Eng. 133 (6), 668–689. http://dx.doi.org/10.1061/(ASCE)0733-9429(2007)133:6(668).

Van Rijn, L., Grasmeijer, B., Perk, L., 2018. Effect of channel deepening on tidal flow and sediment transport: part I - sandy channels. Ocean Dyn. 68 (11), 1457–1479. http://dx.doi.org/10.1007/s10236-018-1204-2.

Van Rijn, L., Reniers, A., Zitman, T., Ribberink, J., 1995. Yearly-averaged sand transport at the -20 m and -8 m NAP depth contours of the JARKUS-profiles 14, 49, 76 and 103. Report H1887. Technical Report, WL|Delft Hydraulics, Delft, The Netherlands, p. 101.

Zijl, F., Veenstra, J., Groenenboom, J., 2018. The 3D Dutch Continental Shelf Model - Flexible Mesh (3D DCSM-FM). Setup and validation. Report 1220339-000-ZKS-0042. Technical report, Deltares, Delft, The Netherlands.